Experimental study of launched ion-acoustic waves in a plasma using continuous wave CO2 laser scattering

Experimental study of launched ion-acoustic waves in a plasma using continuous wave CO_2 laser scattering

P. BRODEUR, H. W. H. VAN ANDEL, D. C. SCHRAM,[1] AND V. M. M. GLAUDE
Département de Physique, Université de Montréal, Montréal, Qué., Canada H3C 3J7

Received December 17, 1982

A study of coherent density fluctuations in a low density plasma using continuous wave CO_2 laser scattering diagnostics is reported. A simple and direct description of collective scattering theory from monochromatic electrostatic waves is presented. The diagnostic technique is described in detail and its performance is analyzed. Experimental results on externally launched ion-acoustic waves are presented and it is demonstrated that accurate measurements of certain plasma parameters are possible.

Une étude des fluctuations cohérentes de densité dans un plasma de faible densité avec le diagnostic de la diffusion laser CO_2 continu est rapportée. Une description simple et directe de la théorie de la diffusion collective provenant des ondes électrostatiques monochromatiques est présentée. La technique de diagnostic est décrite en détail et ses performances sont analysées. Des résultats expérimentaux sur des ondes iono-sonores artificiellement émises sont présentés et il est démontré que la mesure précise de certains paramètres du plasma est possible.

Can. J. Phys. **61**, 1231 (1983)

1. Introduction

Coherent scattering of continuous wave (C.W.) CO_2 and far-infrared laser beams has been used in many laboratories to study fluctuations and wave phenomena in plasmas. Studies have been carried out in various types of plasmas for the diagnosis of both spontaneously occurring fluctuations and launched waves. Measurements of spontaneously occurring fluctuations in toroidal confinement machines using laser scattering have been published by various authors (1–4). These are of great importance for the understanding of plasma turbulence leading to anomalous loss of plasma confinement. Scattering studies of turbulence in arc plasmas (5, 6) have been carried out to give information on fundamental processes occurring in these plasmas. Also, laser scattering has been used to study the propagation and conversion of waves launched in toroidal plasmas for heating purposes (7, 8). Finally, the measurement of propagation characteristics of small amplitude waves artifically created in a plasma has been carried out by a number of authors to study wave dispersion and to improve and further develop scattering techniques (9–11).

Because C.W. laser scattering gives, in principle, a very detailed and accurate measurement of the propagation of launched waves in plasmas, it has been shown that such measurements can in fact serve as a diagnostic technique for the measurement of plasma parameters (12). Such a measurement is possible provided the wave dispersion and/or attenuation is a known function of the plasma parameters to be determined, and the wave parameters can be measured to sufficient accuracy using the scattering method. A high degree of accuracy can be readily obtained using phase-sensitive techniques made possible because the waves are externally launched.

It is the purpose of this contribution to report on the use of a CO_2 laser scattering system to study the propagation of launched ion waves in a low density plasma, and to demonstrate that accurate measurements of certain plasma parameters are possible using this technique even in low density plasmas. The scattering system used was developed for future use on the Varennes Tokamak (13), now under construction. Its use in the study of launched waves has not only shown the possibility of plasma parameter diagnostics, but also permits a detailed study of the limits and resolution of this diagnostic technique.

In what follows, we first present, in Sect. 2, a simple and rather direct theoretical description of the theory of laser scattering from monochromatic launched electrostatic waves, based on a formalism introduced by Holzhauer and Massig (14). In particular, the description developed here takes into account the spatial variation of the wave amplitude in the plane of the wave front, and also allows a simple analysis of the effect of the precise orientation of the propagation vector of the wave with respect to the direction of the incident laser beam. In Sect. 3, the apparatus and various experimental techniques used in this work are described in detail. The experimental results are described in Sect. 4, while Sect. 5 contains our principal conclusions.

2. Theory

We consider a scattering system geometry as illustrated in Fig. 1. A CO_2 laser beam propagating in the xz

[1]On leave from University of Technology, Eindhoven, The Netherlands.

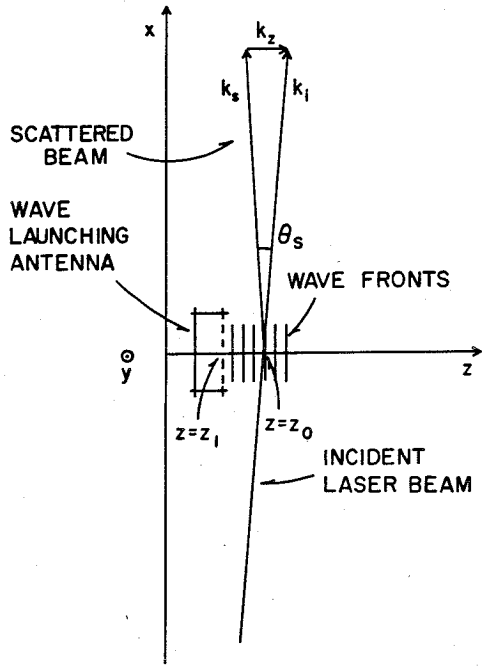

FIG. 1. Schematic diagram of the scattering geometry.

plane in the x direction is scattered at $z = z_0$ from a density perturbation in the plasma. The incident laser beam is assumed to be described by a plane polarized electric field distribution of the form

$$[1] \quad \boldsymbol{E}_i(x,y,z) = y_u E_i(x)\, U_i(x,y,z)$$

where $U_i(x,y,z)$ is the beam profile function, and y_u is the unit vector in the y direction. We assume a detection system which is aligned to measure light scattered in the xz plane at a scattering angle θ_s as indicated in the figure. Provided θ_s is small, we may write

$$[2] \quad \boldsymbol{E}_s(x,y,z) = y_u E_s(x)\, U_s(x,y,z)$$

If the characteristic length Λ in the plasma where scattering takes place is relatively small, we can assume that the incident and scattered beams overlap in this length, and thus we write, for a Gaussian beam,

$$[3] \quad U_i(x,y,z) = U_s(x,y,z) = \exp\left[-\frac{y^2 + (z - z_0)^2}{w^2(x)}\right] \approx \exp\left[-\frac{y^2 + (z - z_0)^2}{w_0^2}\right]$$

where w_0 is half the width of the beam profile at e^{-1} of its maximum amplitude in the plasma. The assumption of beam overlap implies $\Lambda\theta_s \ll w_0$.

We consider the situation where the scattered light is detected using the well-known method of "homodyne" optical mixing. Here the scattered beam is mixed with a local oscillator taken from the incident laser beam and rendered colinear to the scattered beam by suitable optical means (see Fig. 3). Under these conditions, we may use the result of Holzhauer and Massig (14), and write the intermediate frequency detector current as

$$[4] \quad i_{if}(t) = \frac{2j\alpha\xi r_0\lambda_i\sqrt{P_i P_{LO}}}{\pi w_0^2}\int d\boldsymbol{r}\, \tilde{n}_e(\boldsymbol{r},t)\exp\left[-\frac{2(y^2 + (z - z_0)^2)}{w_0^2}\right]\{\exp[-jk_z(z - z_0)] - \exp[jk_z(z - z_0)]\}$$

where $\alpha = \eta e\lambda_i/hc$ is the detector sensitivity, η is the detector quantum efficiency, e is the electronic charge, λ_i is the laser wavelength, h is Planck's constant, c is the velocity of light in a vacuum, ξ is the homodyne mixing efficiency (see Sect. 3), r_0 is the classical electron radius, P_i is the incident laser power, P_{LO} is the local oscillator power, $\tilde{n}_e$ is the density fluctuation amplitude, and $k_z = |\boldsymbol{k}_i - \boldsymbol{k}_s| \approx \theta_s|\boldsymbol{k}_i|$ (see Fig. 1).

We consider the case where $\tilde{n}_e(\boldsymbol{r},t)$ is a plasma fluctuation in the form of a plane wave launched by an antenna (or, equivalently, characterized by a fixed phase) at a position $z = z_1$, and described by

$$[5] \quad \tilde{n}_e(x,y,z,t) = \tilde{n}_{eo}\exp\left[-\frac{x^2 + y^2}{\Lambda^2}\right]\cos(K_x x + K_y y + K_z(z - z_1) - \omega_0 t + \phi)$$

We assume K_x, $K_y \ll K_z$, but not necessarily equal to zero. Therefore, the effect of a slight misalignment of the wave fronts with respect to the beam direction can be studied. Also, we have chosen a Gaussian amplitude profile in the plane of the wave front of characteristic width Λ in order to study the effect of the finite extent of the wave.

Substitution of [5] in [4], and subsequent integration gives

$$[6] \quad i_{if}(t) = \frac{\sqrt{\pi}\tilde{n}_{eo}\alpha\xi r_0\lambda_i\Lambda^2\sqrt{P_i P_{LO}}}{\sqrt{\Lambda^2 + w_0^2/2}}\sin[K_z(z_0 - z_1) - \omega_0 t + \phi]\exp\left[-\frac{K_x^2\Lambda^2}{4}\right]\exp\left[-\frac{K_y^2 w_0^2\Lambda^2}{4(2\Lambda^2 + w_0^2)}\right] \times\left\{\exp\left[-\frac{(k_z - K_z)^2 w_0^2}{8}\right] - \exp\left[-\frac{(k_z + K_z)^2 w_0^2}{8}\right]\right\}$$

There are a number of features of this result which are of interest for the experimental procedure and interpretation used in scattering measurements from coherent launched waves. First we note that the detector current is maximum for $k_z = \pm K_z$. This means that the method cannot distinguish between waves which propagate in the positive and negative z directions. Thus, the scattering signal is maximum at $\theta_s = \pm K_z\lambda_i/2\pi$. The resolution in K_z is given by the exponential form factor: if we define ΔK_z by the e^{-1} point of the i.f. current amplitude, we find $\Delta K_z = \sqrt{8}/w_0$; this corresponds to a range of scattering angles $\Delta\theta_s = \Delta K_z/k_i = \sqrt{2}\lambda_i/\pi w_0$.

A careful adjustment of the scattering angle to maximum amplitude gives a measure of K_z associated with the wave. However, an independent and potentially more accurate method of determining K_z can be employed by making use of the sinusoidal phase factor $\sin(K_z(z_0 - z_1) - \omega_0 t + \phi)$ in [6]. First, this phase factor predicts that the scattering signal occurs at the frequency ω_0 which is the frequency associated with the launched wave. The quantity $(K_z(z_0 - z_1) + \phi)$ adds a phase angle which is fixed provided z_0, z_1, and ϕ are fixed. If, however, either z_0 (the laser position) or z_1 (the launching antenna position) is varied, it is possible to vary this phase angle. This result suggests the use of a phase sensitive detection system tuned to ω_0. A continuous variation of z_1, for example, then allows a continuous variation of the phase of the wave. By sweeping through a distance $|z_0 - z_1|$ which is several times $2\pi/K_z$, an accurate measurement of K_z can be made. This measurement is independent of the exact alignment of the system provided sufficient signal is intercepted to allow the phase-sensitivie detection. Additional benefits of this method are that the signal-to-noise ratio associated with the detection scheme can be increased significantly and the optical alignment can be optimized very simply.

The exponential factors involving K_x and K_y show the effects of a wave propagation vector which is not strictly parallel to the z axis. We note that a small deviation of $\boldsymbol{K}$ in the x direction gives a much sharper decrease in signal than a corresponding deviation in the y direction. If we denote by ΔK_x and ΔK_y the e^{-1} points of the exponential factors associated with the corresponding "misalignments" of the wave vector, we find $\Delta K_x = 2/\Lambda$ and $\Delta K_y = 2\sqrt{2\Lambda^2 + w_0^2}/w_0\Lambda$. In a typical experimental situation $w_0 \ll \Lambda$, therefore, $\Delta K_y \approx 2\sqrt{2}/w_0$. We define the angles of nonalignment corresponding to ΔK_x and ΔK_y by $\Delta\phi_x = \Delta K_x/K_z$ and $\Delta\phi_y = \Delta K_y/K_z$, respectively. We then obtain $\Delta\phi_x = 2/\Lambda K_z$ and $\Delta\phi_y = 2\sqrt{2}/w_0 K_z$. It is clear that for $\Lambda \gg w_0$, the alignment in the x direction is much more critical than the alignment in the y direction. Physically this means that when Λ is relatively large, a small misalignment of the wave with respect to the direction of the laser beam will cause destructive interference of neighboring wave fronts over the effective scattering length. If a possibility exists to experimentally change K_x and K_y (for example by turning a launching antenna), it is possible to determine Λ and w_0 by measuring the corresponding variations in the detector current. Also, a measure of the effective coherence length of the wave fronts may be made as a function of distance from the launching antenna. This can give information about the wave front spreading and curvature.

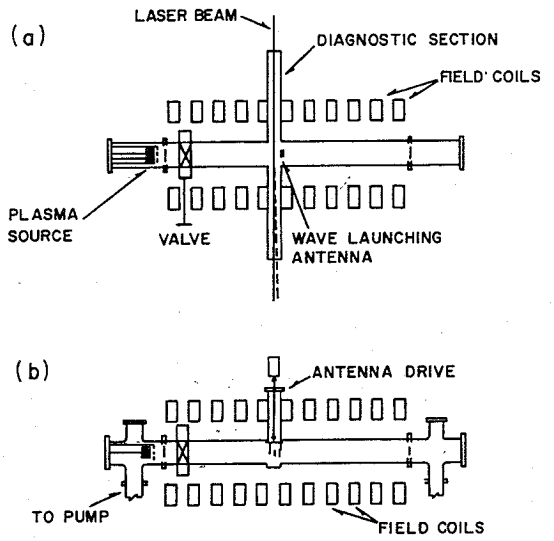

FIG. 2. Schematic diagram of the plasma machine and associated systems; (a) plan view; (b) front elevation.

The constant factor in [6] allows a determination of the absolute value of the fluctuating part of the electron density $\tilde{n}_{eo}$. Assuming the system is aligned so that $K_x = K_y = 0$ and $\theta_s = K_z\lambda_i/2\pi$, then all the exponential factors are equal to 1, and we have, for $\Lambda \gg w_0$:

$$[7] \quad \langle i_{if}^2 \rangle = \frac{1}{2}\pi\Lambda^2\tilde{n}_{eo}^2\alpha^2\xi^2 r_0^2\lambda_i^2 P_i P_{LO}$$

We note that for homodyne optical mixing of a local oscillator of power P_{LO} with a scattered power P_s with mixing efficiency ξ, the intermediate frequency current is given by (15):

$$[8] \quad \langle i_{if}^2 \rangle = 2\alpha^2\xi^2 P_{LO} P_s$$

Thus, combining [7] and [8] gives, for the total scattered power,

$$[9] \quad P_s = \frac{\pi}{4}\tilde{n}_{eo}^2\Lambda^2 r_0^2\lambda_i^2 P_i$$

This result is the same as that given by Surko and Slusher (2) for an effective scattering length $\sqrt{\pi}\Lambda$. Provided α, ξ, P_i, P_{LO}, Λ, and $\langle i_{if} \rangle_{RMS}$ can be measured

(see Sect. 3), one can obtain $\tilde{n}_{eo}$ from [7].

3. Experimental apparatus and procedures

In this section we describe the various components of the experimental arrangement, as well as a number of the procedures followed to prepare and calibrate the system for the measurements described in Sect. 4.

A. Test plasma

The plasma used for the scattering studies consists of a weakly ionized column in argon created by a hot cathode plasma source at one end. The plasma is allowed to diffuse freely away from the hot cathode source along the axis of a 10 cm radius stainless steel tube. An axial magnetic field applied externally effects radial confinement and allows the creation of a long plasma column. Figure 2 shows a schematic diagram of the experimental arrangement which is similar to that used and described in a previous publication (16). The plasma source consists of an indirectly heated oxide-coated cathode of 9 cm diameter together with a grounded gridded anode which is placed 3 cm from the cathode surface. When a negative potential is applied to the heated cathode, a plasma is created which can freely diffuse through the gridded anode. The parameters of the plasma source and column are summarized in Table 1. The plasma parameters are measured using Langmuir probes.

As shown in Fig. 2, about 1 m downstream from the cathode a diagnostic section is constructed for the scattering measurements. It consists of two horizontal stainless steel side arms of rectangular cross section fitted at the ends with large rock-salt windows 2.5 cm thick. These are placed at the Brewster angle to reduce unwanted reflections of the laser beam. A side arm in the third direction contains moveable mounts for antennas and probes which can be inserted in the plasma to launch and diagnose ion-acoustic waves. A piezoelectric crystal may also be mounted there to create acoustic waves in air.

TABLE 1. Summary of experimental parameters

Plasma parameters	
Gas	Argon
Neutral pressure	$\sim 10^{-3}$ Torr
Electron temperature	1–4 eV
Electron density	$1-5 \times 10^{16}$ m^{-3}
Magnetic field	100–300 G
f_{pe}	~1 GHz
f_{pi}	~5 MHz
λ_{Debye}	~0.5 mm
v_{the}	$\sim 5 \times 10^5$ m s^{-1}
Ion-acoustic speed	$\sim 2 \times 10^3$ m s^{-1}
Wave excitation	
Grid mesh	80/cm stainless steel
Excitation	~1–5 V peak to peak
Bias	−60 V
Back plate at 5 mm	Grounded
Diameter	2 cm
Detector parameters	
Type	HgCdTe (SAT) Photovoltaic
Area	4×10^{-4} cm^2
Operating temperature	77 K
Bandwidth	290 MHz
Responsivity α	1.8 A W^{-1}
Bias	−0.5 V
Maximum power dissipation	14 mW
Coupling to amplifier	rf transformer $N_1/N_2 = 2$
Quantum efficiency	0.21 at 10.6 μm
Optical link	
Type	Meret (Analog)
Bandwidth	direct current — 25 MHz
Input impedance	50 Ω
Plasma source	
Type:	Indirectly heated cathode with acceleration grid
Heater power	1 KW alternating current
Cathode surface temperature	1050°C
Cathode diameter	9 cm
Cathode–grid spacing	3 cm
Grid accelerating voltage	30 V
Cathode–grid current	4A
Laser parameters	
Type	CO_2 single L/T mode
Power	5–10 W continuous
Beam divergence	1.9 mrad
Wavelength	10.6 μm
Amplifier	
Type	Avantek
Gain	27 dB
Input impedance	50 Ω
Noise figure	2 dB
Bandwidth	0.001–500 MHz
Lock-in amplifier	
Bandwidth	0.1–50 MHz
Max. sensitivity	10 μV full scale
Input impedance	50 Ω

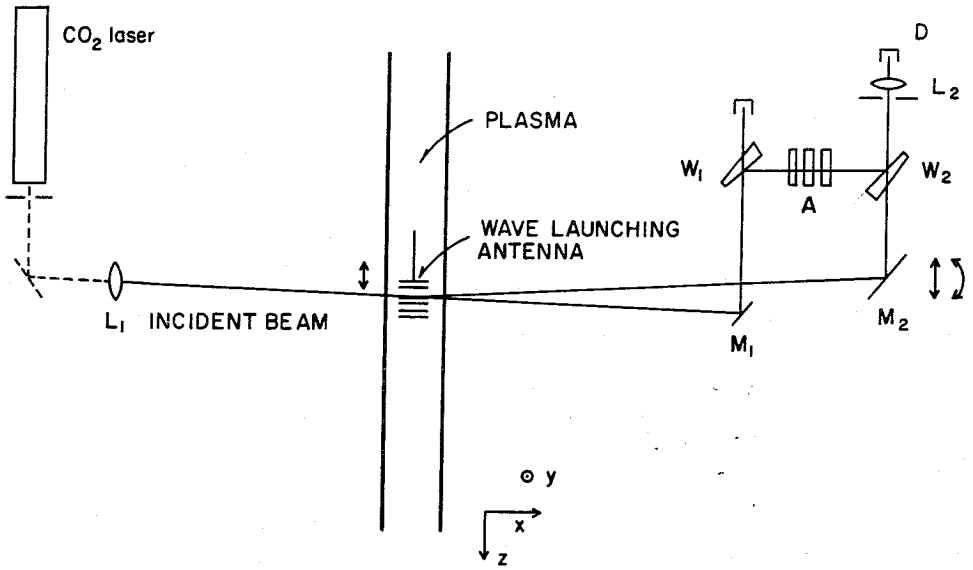

FIG. 3. Arrangement of the optical system used for the scattering measurements.

B. Wave generation and probe measurement

The antenna used to launch the ion waves consists of a 2 cm diameter grid with a 2 cm diameter backing plate 5 mm from the grid. This design was inspired by experiments done by Sessler (17) on ion-acoustic wave production in plasmas. The backing plate is grounded and an oscillating signal is applied to the grid which is negatively biased.

A simple Langmuir probe can be inserted in the plasma to monitor the plasma wave created by the launching antenna. Various mechanisms in the antenna and probe mounts allow calibrated independent displacement of the launching antenna and the probe in both axial (z) and radial (y) directions (see Fig. 3) over a range of about 6 cm. A calibrated rotation of the antenna surface about the y axis can also be performed.

The antenna is driven by an oscillating signal whose frequency may be varied between 100 kHz and 10 MHz. When a probe is used to study the resulting wave, we make use of what is basically a probe interferometer system. The signal applied to the antenna is also applied to the reference input of a high frequency lock-in amplifier (PAR 5202). The probe signal, after suitable amplification if necessary, is applied to the signal input. In this mode, the lock-in amplifier acts as a phase-sensitive detector; both the in phase and quadrature components of the signal with respect to the reference are available at the lock-in output. This allows direct measurement of the signal amplitude. Because the phase of the signal on the receiving probe depends on its position with respect to the launching antenna, a continuous displacement of the probe with respect to the antenna allows a sweep through several wavelengths of the launched wave. The in-phase signal is then displayed on the Y axis of an $X-Y$ recorder whose X axis is driven by a signal proportional to the probe position. This effectively gives a trace of the instantaneous wave amplitude as a function of position.

C. Laser scattering system

Figure 3 shows a schematic diagram of the laser scattering system as used in this experiment. A CW CO_2 laser of maximum power 10 W (MPB Technologies) produces a beam characterized by a single longitudinal and transverse mode. The laser is fitted with a 2 m radius of curvature concave grating at the closed end which allows the selection of a single spectral line output. For our experiment the laser was tuned to 10.6 μm (P-20 line of CO_2). A Lansing piezoelectric stabilizing system is installed at the output mirror end to lock the laser to the maximum amplitude of a single longitudinal mode. An iris is placed inside the optical cavity near the output to eliminate all transverse modes except the fundamental transverse electromagnetic $(TEM)_{00}$ mode. A pyroelectric power meter is used to monitor the laser power. Using a small pinhole and this power meter, the beam intensity profile is measured giving at the laser output an elliptical beam profile having a waist radius w of 1.37 mm parallel and 2.14 mm perpendicular to the direction of polarization. The beam is plane polarized in the horizontal direction at the laser output. The laser is placed at a lower level than the plasma levels and is first deviated upwards and then horizontally into the plasma using two gold-plated mirrors. This arrangement allows a vertical displacement of the laser beam in the plasma without moving the laser, and also changes the direction of polarization from horizontal to vertical. A 91 cm focal length lens L_1

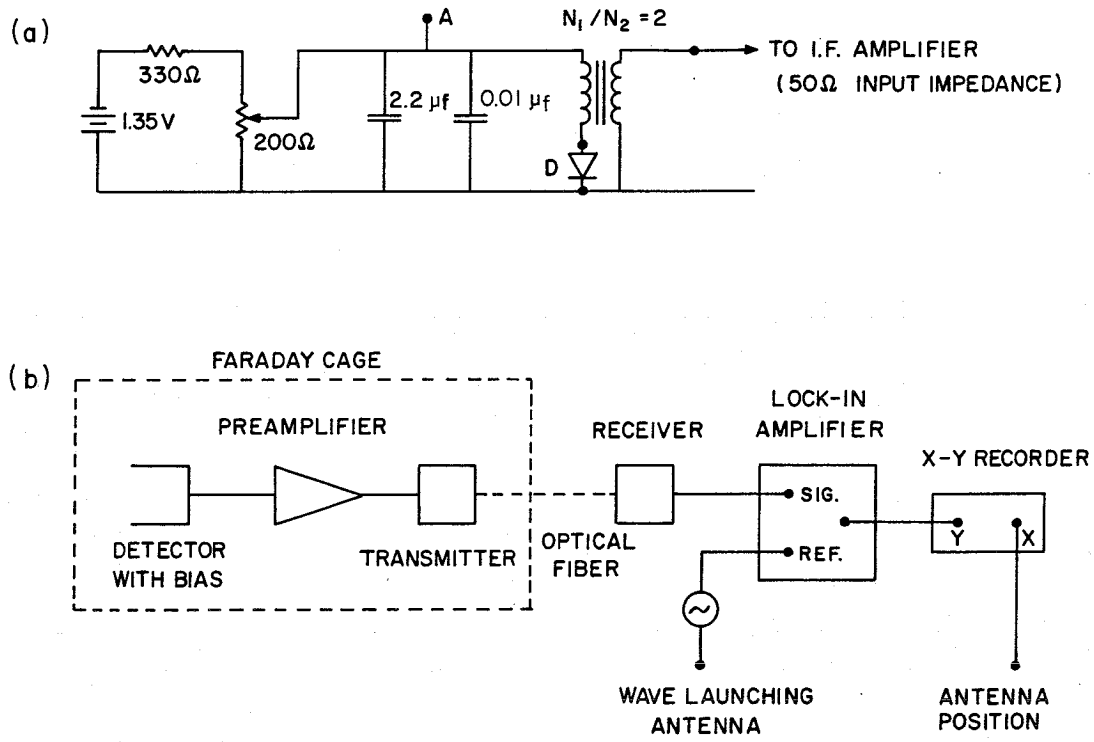

FIG. 4. (a) Details of the detector circuit. (b) Block diagram showing scattering signal detection system.

is used to focus the beam in the centre of the plasma column. The corresponding waist half width w_0 at the plasma was 1.45 ± 0.05 mm in the direction perpendicular to the plane of polarization (z direction). Subsequent to scattering, the unscattered and scattered beams follow paths as indicated in Fig. 3. The unscattered beam, whose intensity is not diminished very much, is deviated by a small mirror M_1 onto a salt wedge W_1. The majority of the beam energy passes through W_1 onto a beam dump. A small fraction of the beam incident on W_1 is reflected and further attenuated by CaF_2 absorbers of various thickness (1–8 mm) used to control the beam intensity. The attenuated beam is then reflected by a salt wedge W_2 onto the detector via the lens L_2 whose focal length is 5 cm. This beam represents the local oscillator invoked in Sect. 2. The scattered beam bypasses the mirror M_1 and is reflected by mirror M_2 onto the wedge W_2. The lateral position of M_2, as well as its inclination, can be adjusted so that for a given scattering angle, the scattered beam is rendered colinear with the local oscillator beam and focussed onto the detector where optical mixing takes place. The 5 cm focal length lens produces a focal spot on the detector surface whose size is diffraction limited, in the order of 100 μm in radius.

The detector used is a Société Anonyme de Télécommunications (SAT) HgCdTe photovoltaic diode of active dimension 0.2×0.2 mm^2, and is cooled to 77 K. The detector is biased negatively in order to effect its operation at an operating point characterized by a large reverse resistance. The detector circuit is shown in Fig. 4a, with the detector designated by the symbol D. Coupling to the post detection electronics is achieved using a small radio frequency (rf) transformer having a turns ratio of 2:1. The signal is fed to a wide-band low-noise Avantek amplifier of gain 27 db. For very weak signals, two such amplifiers may be used in series. The amplified signal is then fed to the lock-in amplifier as shown in Fig. 4b. In order to reduce unwanted electrical pickup on the detector circuit, the detector and amplifier were enclosed in a Faraday cage. An optical analog link was used to transmit the signal to the lock-in amplifier. Inside the Faraday cage, all power requirements were met using batteries. Because the homodyne detector signal is at frequency ω_0 associated with the plasma wave, phase sensitive detection is possible using the signal on the wave-launching antenna as a reference. As explained in Sect. 2, the phase difference of the i.f. detector signal with respect to the launching signal may be varied by moving the launching antenna with respect to the laser beam; this gives a direct measurement of the wavelength of the plasma wave provided the optics are aligned to receive a signal near the appropriate scattering angle. As shown in Fig. 4b, the output of the lock-in amplifier is displayed on the Y axis of an $X-Y$ recorder, X representing the pos-

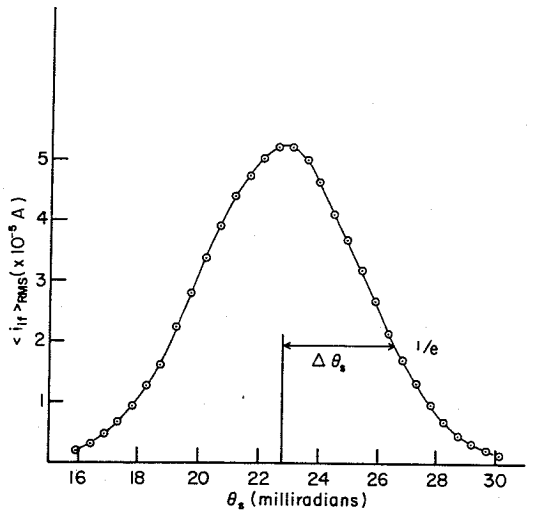

FIG. 5. Plot of the RMS detector current as a function of scattering angle for scattering from a pressure wave in air of fixed frequency and wavelength (f = 750 kHz).

ition of the launching antenna with respect to the laser beam. The characteristics of the entire detection system are summarized in Table 1.

Because interferometric measurements of the type described are particularly sensitive to mechanical vibrations, the entire optical system was mounted on vibration-damping isolators.

D. Noise considerations

The homodyne detection method described is particularly effective in increasing the effective signal-to-noise ratio associated with the scattered power detection. Provided the local oscillator power is sufficiently large so as to create shot noise in the detector which exceeds all other sources of noise, the theoretical signal-to-noise ratio, including post-detection averaging, is given by (15):

$$[10]\quad \frac{\langle i_{if}^2\rangle}{\langle i_N^2\rangle} = \frac{\eta\xi^2\lambda_i P_s}{hcB}$$

where B is the effective detection bandwidth. Assuming the signal to be narrow compared to a post-detection filter bandwidth Δf, and assuming an integration time τ associated with the lock-in detection technique, we have $B = (\Delta f/\tau)^{1/2}$. For our lock-in amplifier, $\Delta f \sim 100$ Hz and $\tau = 1$ s. This gives $B = 10$ Hz. Thus, the noise equivalent power is equal to $hcB/\eta\lambda_i\xi^2 \approx 10^{-18}$ W.

E. Calibration procedures

A first alignment was performed using a He–Ne laser and a small slit placed at the scattering position. The diffraction pattern from the slit was used to simulate scattering at various angles, and thus the scattering optics could be approximately aligned.

In order to calibrate the optical alignment more accurately and also to study the resolution and detection procedures, a piezoelectric crystal was used to launch acoustic waves in air. The laser beam is scattered in the air by the pressure wave, and this method provides a very effective way of simulating the scattering which occurs from a plasma wave. The advantage of using this pressure transducer is that the waves which are produced are attenuated very little, have well-defined plane wave fronts, and produce strong scattering signals. The crystal used was a Valpey-Fisher model with a 1.9 cm diameter and a measured resonant frequency of 700 kHz. It was operated in the 0.4–1 MHz range. The corresponding wavelengths in air for acoustic waves could be varied from 0.35 mm to 0.9 mm, allowing calibration and alignment of the system over a range of scattering angles from 12 to 30 mrad. Because the calibration is linear, we were able to extrapolate to smaller and larger scattering angles. In this way reproducible settings of the position and inclination of the mirror M_2 could be found for the maximum i.f. current signal as a function of K_z corresponding to the acoustic wave in air. The scattering angle could be calibrated in this way to a precision of ± 0.1 mrad. The signals were processed using the phase-sensitive detection method described earlier. The accuracy of this method is illustrated by the fact that a determination of the speed of sound in air based on these measurements gave a value of 350 ± 3 ms^{-1}; the published value for dry air at our room temperature is 346.2 ms^{-1}.

The acoustic crystal was also used to determine the K_z resolution, the loss in signal due to misalignment of the launching antenna, and the mixing efficiency. These will now be discussed in turn.

For determination of the K_z resolution (see Sect. 2), a wave was launched at fixed frequency (i.e., fixed K_z) and the angle at which the signal was detected was varied using the calibrated settings of M_2 as described earlier. The resulting i.f. detector current variation with θ_s is shown in Fig. 5. The e^{-1} points gave a value of $\Delta\theta_s$ of 3.80 ± 0.05 mrad corresponding to a ΔK_z of 2.25×10^3 m^{-1}.

Based on the theoretical prediction of the K_z resolution given in Sect. 2 and the measured beam profile in the scattering volume, we would predict $\Delta K_z = 1.95 \times 10^3$ m^{-1}. This is slightly smaller than the measured value using the acoustic waves in air. Although these waves appear to be hardly damped in the measurements, it is possible that they exhibit some broadening in K space. This translates to an apparent instrumental resolution which is slightly worse than the theoretically predicted value. Noting that the value of K_z for the measurements presented in Fig. 5 is 1.34×10^4 m^{-1}, we have $\Delta K_z/K_z = 0.168$ which is a fairly good resolu-

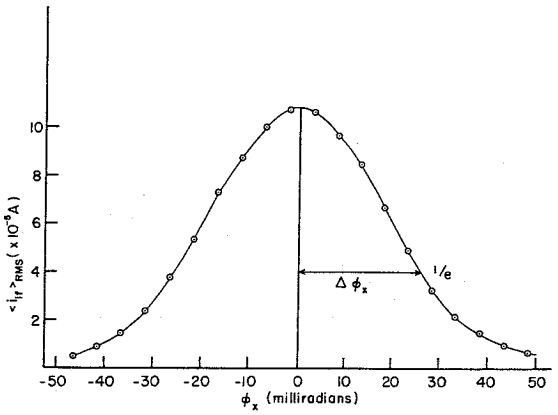

FIG. 6. Plot of the RMS detector current as a function of $\phi_x \equiv K_x/K_z$ for scattering from a pressure wave in air of fixed frequency and wavelength (f = 700 kHz, θ_s = 21 mrad, $K_z = 1.24 \times 10^4$ m^{-1}, $(z_0 - z_1)$ = 1 cm).

tion considering the scattering angle θ_s is about one degree. Of course ΔK_z is not a function of θ_s, and thus the resolution becomes progressively worse at smaller scattering angles.

The effect of the direction of the wave vector of the launched waves with respect to the laser beam direction was studied by rotating the piezoelectric crystal about a diameter parallel to the y axis (see Fig. 1). In this way a variable propagation vector component K_x can be introduced, and [6] predicts a corresponding variation of the i.f. detector current. Figure 6 shows a measurement of the i.f. detector current at a fixed scattering angle as a function of $\phi_x \equiv K_x/K_z$. We note that the curve is Gaussian in shape, with the e^{-1} width given by $\Delta\phi_x = 25.1 \pm 0.5$ mrad. Using the results developed in Sect. 2, we find $\Delta K_x = 3.2 \times 10^2$ m^{-1} which implies $\Lambda = 6.3 \times 10^{-3}$ m. (Λ is the characteristic length of the amplitude profile of the waves (see [5]).) This measurement was made with a crystal of 0.95 cm radius. An important conclusion to be drawn from this measurement is that only those K vectors within a small range of ϕ_x can be observed if the wave fronts have significant spatial extent in the direction perpendicular to the wave vector, parallel to the laser beam.

The transducer was also used to determine the mixing efficiency ξ which is a measure of the matching of wave fronts in the homodyne mixing process (15, 2). When the transducer is energized with a relatively large oscillating potential, the scattered power becomes so large that it can be measured directly without using the homodyne mixing techniques, provided an optical chopper and low frequency lock-in amplifier is used. The corresponding detector current, which can be found by measuring the potential at point A on Fig. 4a, is given by $i_s = \alpha P_s$. If we measure the detector current

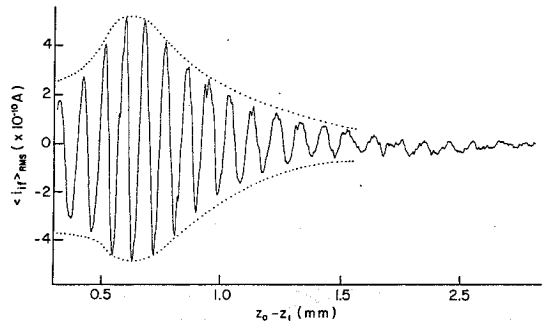

FIG. 7. Plot of the in-phase component of the RMS detector current as measured by the lock-in amplifier as a function of position of the wave-launching antenna relative to the laser beam, showing the periodic variation of the plasma wave amplitude as a function of position in the plasma (f = 1.8 MHz, θ_s = 13 mrad).

due to the local oscillator power only, we have $i_{LO} = \alpha P_{LO}$. Combining these results with the expression given in [9] for the homodyne i.f. current, we obtain

$$[11] \quad \xi = \frac{\langle i_{if} \rangle_{RMS}}{\sqrt{2 i_s i_{LO}}}$$

Using calibrated measurements of i_s, i_{LO}, and $\langle i_{if} \rangle_{RMS}$ for the same scattering situation, we found $\xi \sim 0.7$ for the best possible alignment.

When scattering measurements are made at $\theta_s <$ 6 mrad, a significant portion of the unscattered beam passes via mirror M_2 onto the detector. This part of the beam acts as a local oscillator and in principle does not affect the measurements. However, as θ_s is further decreased, the amount of power due to the wings of the main beam increases very rapidly with great risk to the detector. Also, when a significant fraction of the local oscillator power comes via M_2, it is more difficult to distinguish true scattering signals from spurious effects. For this reason scattering angles below 6 mrad were not used in this mode of operation, thus limiting our measurements to wavelengths less than 2 mm.

4. Measurements on plasma ion-acoustic waves

The laser scattering system was used to study ion-acoustic waves launched in the plasma using the launching antenna described in the previous section. We were able to launch ion waves in the frequency range 100 kHz−10 MHz, depending on the plasma conditions. Figure 7 shows a typical plot of $\langle i_{if} \rangle_{RMS}$ as a function of the launching antenna position (i.e., as a function of $(z_0 - z_1)$, see [6]), using the phase-sensitive lock-in technique described in Sect. 3. The frequency of the launched wave for this measurement was fixed at 1.8 MHz, and the scattering angle was 13 mrad, which corresponds to $K_z = 7.7 \times 10^3$ m^{-1} and thus a wave-

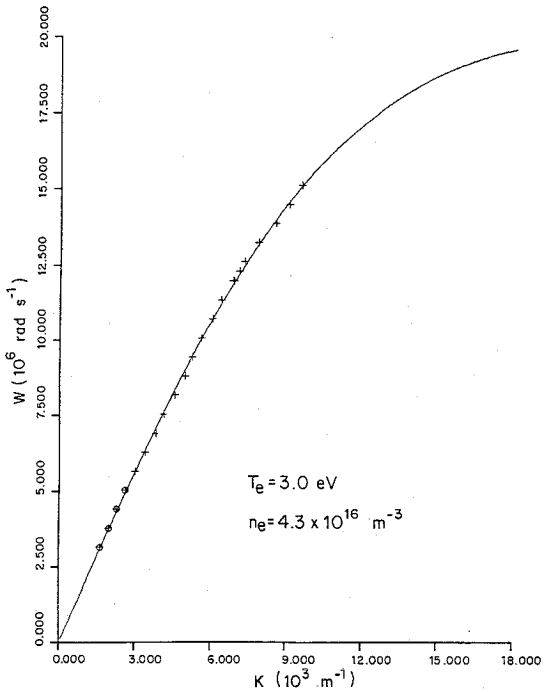

FIG. 8. Dispersion curve for ion acoustic waves obtained using laser scattering measurements (+) and probe measurements (○). The solid line is a best fit based on [12], using T_e and n_e as free parameters, and assuming $T_i = 0.06$ eV and $V = 0.85$ km s^{-1}. The resulting values of T_e and n_e are shown.

length of 0.82 mm. As can be determined from Fig. 7, the wavelength varies slightly over the length of the sweep made; near the antenna the wavelength is slightly larger. It decreases and then increases again at larger distances. The amplitude variation is probably the result of a number of competing factors. The increase in signal amplitude at small values of $(z_0 - z_1)$ could be due to the fact that the wave experiences spatial growth as a result of fast electrons emitted from the negatively biased launching antenna. Various damping mechanisms (see subsequent discussion) cause a reduction in the signal at larger values of $(z_0 - z_1)$. Also, the small variations in wavelength give changes in amplitude because the scattering angle for this measurement is fixed, and only optimal in the range $(z_0 - z_1) \approx 0.6$ cm. Using a measured resolution curve for fixed θ_s and varying K_z, we were able to correct for this small effect (dotted line).

By repeating traces such as shown in Fig. 7 for different frequencies for the same plasma conditions, it is possible to obtain the dispersion relation for ion-acoustic waves with a great deal of accuracy. For each trace the scattering angle was chosen as predicted by the theoretical dispersion relation, assuming values of T_e and n_e given by previous measurements. The wavelength for each frequency was measured in the same range of $(z_0 - z_1) \sim 1.0$ cm by averaging over about four cycles. Figure 8, where we have plotted ω_0 as a function of the measured K_z, shows a typical result of this type of measurement. Because the wavelength measurement is independent of the exact scattering angle setting (as long as one measures at an angle sufficiently close to the setting for maximum signal so as not to lose too much signal), the wavelength measurement is very easy to perform and can be done with great accuracy.

In order to determine the plasma parameters from the measured dispersion relation, it is necessary to know the theoretical dispersion relation for our plasma. The situation is somewhat complicated by the fact that the plasma as a whole has a flow velocity parallel to the magnetic field which cannot be neglected. This flow velocity is due to the net axial diffusion of the plasma from the source; this diffusion is ambipolar in nature, and electrons and ions diffuse together at a speed which is in the order of a few times the ion thermal speed. The dispersion relation for ion-acoustic waves in the presence of a flow velocity V parallel to K is given by (18)

$$[12] \quad 1 - \sum_{\alpha=e,i} \frac{\omega_{p\alpha}^2}{K^2 a_\alpha^2} \frac{d}{d\xi_\alpha} Z(\xi_\alpha) = 0$$

where $\omega_{p\alpha}$ is the plasma frequency associated with the species α, $a_\alpha = (2\kappa T_\alpha/m_\alpha)^{1/2}$ is the thermal velocity, κ is Boltzmann's constant, and $\xi_\alpha = ((\omega/K) - V)/a_\alpha$. The function $Z(\xi_\alpha)$ is the well-known plasma dispersion function (19).

We were able to determine the flow velocity V by measuring waves launched parallel and antiparallel to V, using electrostatic probes at low frequencies. In this case the phase velocity ω/K changes by a factor $2V$; for the plasma conditions used in the scattering measurements, the result was $V = 0.85 \pm 0.05$ km s^{-1}. The experimental points shown in Fig. 8 were thus fitted to a curve of the form given by [12] using T_e and n_e as free parameters to be determined from the fit. We assumed a fixed value of the ion temperature in our plasma in the order of a few times the room temperature. The curve fitting was done numerically using the phase velocity as an independent parameter and giving all the points approximately equal weight. The resulting curve gave us a measure of T_e and n_e as shown in Fig. 8. This diagnostic technique allows the measurement of both electron temperature and electron density for this type of plasma, and serves as an illustration of the use of laser scattering as a technique for measuring plasma parameters. The value of the ion-acoustic speed $c_s \equiv (\kappa T_e/m_i)^{1/2}$, corresponding to our measured temperature, is 2.68 km s^{-1}; this is the theoretical phase velocity of an acoustic wave at low frequency in the absence of plasma drift. It was clear that V was not

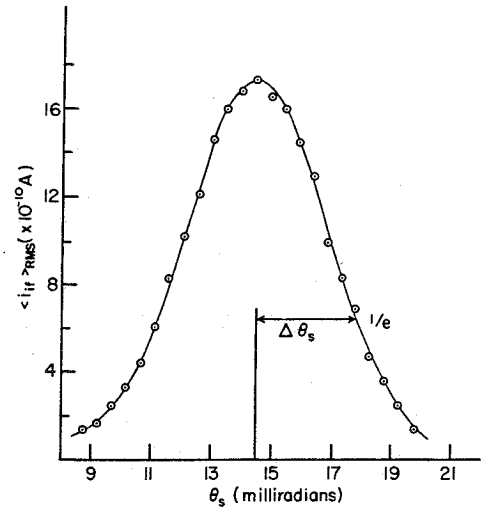

FIG. 9. Plot of the RMS detector current as a function of scattering angle for launched ion-acoustic waves of fixed frequency and wavelength (f = 1.8 MHz).

negligible when compared with c_s; hence the plasma drift needed to be taken into account. For the same plasma conditions, probe measurements as described in Sect. 3 were performed at low frequencies. The resulting points are also shown on the curve in Fig. 8 and give excellent agreement with the scattering measurements.

The fact that the experimental points in Fig. 8 show little scatter around the smooth fitted curve is indicative of the fact that the wavelength measurement can be done with considerable precision. We estimate that the error associated with the lock-in technique for the determination of K_z is typically less than 2% except for those measurements where the signal-to-noise ratio approaches unity (e.g., the last two points on the curve). There it may be somewhat larger. It is of interest to estimate the error in the derived parameters T_e and n_e, assuming [12] accurately represents the wave dispersion. The program used for curve fitting does not give this error explicitly, but it can be estimated from the scatter of the points on the curve and the theoretical dependence of ω/K on T_e and n_e. Thus an empirical approach was followed where we determined to what extent the fitted values of T_e and n_e depend on the precise values of the input parameters of the computer program, i.e., ω/K, V, and T_i. By assuming random errors in the values of ω/K and V up to $\pm 5\%$, and an error in the assumed value of T_i up to $\pm 50\%$, we were able to determine that these errors would introduce errors in the fitted value of T_e up to $\pm 5\%$, and in the fitted value of n_e up to $\pm 15\%$. Because the errors in ω/K, V, and T_i should be within the above bounds, we estimate that our determined values of T_e and n_e are correct to within 5 and 15% respectively, assuming [12] correctly describes the wave which we have observed.

It is of interest to determine to what extent the waves are monochromatic in the plasma, i.e., to determine if a single frequency wave produces waves over a range of K. To this end the K_z resolution experiment performed with the piezoelectric crystal described in Sect. 3 was repeated using the ion wave launcher. The result is shown in Fig. 9. From this result we deduce that there is no measurable broadening; the measured ΔK_z is equal to 1.96×10^3 m^{-1}; this is very close to the theoretical value of $\Delta K_z = 1.95 \times 10^3$ m^{-1} based on the measured value of w_0 in the scattering volume.

As shown in [7], it is possible to calculate the absolute value of $\tilde{n}_{eo}$ from a measurement of the RMS detector current. We have

$$[13] \quad \tilde{n}_{eo} = \left\{ \frac{2\langle i_{if}^2 \rangle}{\pi(\Lambda\alpha\xi r_0 \lambda_i)^2 P_i P_{LO}} \right\}^{1/2}$$

We can experimentally determine all the quantities appearing in [13]. Λ is determined from a variation of i_{if} with K_x as explained in Sect. 3; we performed this measurement for the ion-acoustic waves launched by our antenna and found Λ = 3.5 mm at the position where the measurements were taken. The quantity $\alpha \equiv \eta e \lambda_i / hc$ is the detector sensitivity in units of current per incident power; it may be simply calculated using the manufacturer's quoted value for the detector quantum efficiency η; for our detector α = 1.8 AW^{-1}. The mixing efficiency ξ was measured as described in Sect. 3 and has a value of 0.7. P_i can be simply measured using a calibrated power detector, whereas P_{LO} is measured by determining the detector current due to the local oscillator only; in our situation P_{LO} was 0.35 mW. Thus, a measure of $\langle i_{if} \rangle_{RMS}$ gives $\tilde{n}_{eo}$.

We found, using the above values and procedures, that the maximum measured $\tilde{n}_{eo}$ was 2.4×10^8 cm^{-3} which corresponds to $\tilde{n}_{eo}/n_0 \approx 1 \times 10^{-2}$. We found that typically $\tilde{n}_{eo}$ decreased with increasing frequency for launched waves. The smallest observable $\tilde{n}_{eo}$ in this experiment (signal-to-noise ratio ~ 1) corresponded to 7.5×10^6 cm^{-3}. This represents a scattered power of about 10^{-18} W which is the noise equivalent power for this experiment. This is in the same order as the theoretical noise equivalent power calculated in Sect. 3.

In principle, it is possible to study the damping of the wave by noting the variation of amplitude with distance as illustrated in Fig. 7. However, there are a number of factors which make a study of the physics responsible for wave damping difficult. First, it is probable that the wave amplitude profile changes and the wave fronts do not stay perfectly planar as a function of distance from the launcher. These effects translate into a variation of the effective value of Λ which affects the signal strength. Even though the effective value of Λ could be

measured as a function of distance from the launcher, it is questionable if one can simply apply a correction due to this variation. Also, there are slight changes in wavelength which, as noted, give variations in amplitude at a fixed scattering angle. Besides these experimental problems, one has to take into account two damping mechanisms, namely Laudau damping, more important at higher frequencies, and collisional damping (ion-collisions) which is more important at lower frequencies. Hence a determination of physical parameters of the plasma such as ion-temperature or the ion-collision frequency with neutrals is not trivial. Further study is planned on these effects.

5. Conclusions

We conclude that laser scattering measurements on launched waves can give a very accurate determination of the dispersion characteristics of these waves, and consequently may be used for a detailed study of the parameters of the plasma which support the waves. Launched waves can also be used very effectively to study various properties of the scattering system itself, such as K resolution, effects of the directionality of plasma waves, sensitivity, signal-to-noise ratio, and mixing efficiency of the homodyne detection process. These measurements can be made with a great deal of accuracy using phase-sensitive lock-in techniques.

We further conclude that a CO_2 laser scattering system can have sufficient sensitivity so as to make accurate measurements in low density plasma of the kind described in this paper, provided lock-in techniques can be used. In fact, it was demonstrated that coherent density fluctuations with amplitudes as small as 7.5×10^6 cm^{-3} can be observed.

6. Acknowledgements

The authors wish to acknowledge the assistance of Jean-Louis Lachambre and Jochen Meyer in valuable discussions on experimental procedures and techniques. The technical help of François Roy and Robert Lemay and the assistance of Alain Boileau in taking the measurements was much appreciated. This work was supported by the Natural Sciences and Engineering Research Council of Canada and le Ministère de l'Education du Québec.

1. C. M. SURKO and R. E. SLUSHER. Phys. Fluids, **23**, 2425 (1980).
2. R. E. SLUSHER and C. M. SURKO. Phys. Fluids, **23**, 472 (1980).
3. J. MEYER and C. MAHN. Phys. Rev. Lett. **46**, 1206 (1981).
4. P. LEE, N. C. LUHMANN, JR., H. PARK, W. A. PEEBLES, R. J. TAYLOR, and C. X. YU. Appl. Opt. **21**, 1738 (1982).
5. B. F. M. POTS, J. J. H. COUMANS, and D. C. SCHRAM. Phys. Fluids, **24**, 517 (1981).
6. J. L. LACHAMBRE, R. DECOSTE, and H. W. H. VAN ANDEL. Bull. Am. Phys. Soc. **27**, 1053 (1982).
7. R. E. SLUSHER, C. M. SURKO, J. J. SCHUSS, R. R. PARKER, I. H. HUTCHINSON, D. OVERSKEI, and L. S. SCATURRO. Phys. Fluids, **25**, 457 (1982).
8. P. LEE, N. C. LUHMANN, JR., A. MASE, W. A. PEEBLES, A. SEMET, and S. J. ZWEBEN. Nucl. Fusion Suppl. 2, 68 (Part C) (1981).
9. A. L. PERATT, R. L. WATTERSON, and H. DERFLER. Phys. Fluids, **20**, 1900 (1977).
10. H. PARK, W. A. PEEBLES, A. MASE, N. C. LUHMANN, JR., and A. SEMET. Appl. Phys. Lett. **37**, 279 (1980).
11. G. WURDEN. Ph.D. dissertation. Princeton University, Princeton, NJ. 1982.
12. G. A. WURDEN, M. ONO, and K. L. WONG. Phys. Rev. A, **26**, 2297 (1982).
13. P. COUTURE, J. GEOFFRION, B. C. GREGORY, H. W. H. VAN ANDEL, R. A. BOLTON, P. B. CUMYN, B. L. STANSFIELD, B. TERREAULT. Proc. 19th Symp. Eng. Probl. Fusion Res. Chicago, IL. 1981. Paper 65-26.
14. E. HOLZHAUER and J. H. MASSIG. Plasma Phys. **20**, 867 (1978).
15. O. DELANGE. IEEE Spectum, **5**, No. 10, 77 (1968).
16. C. BOUCHER, S. Q. MAH, H. W. H. VAN ANDEL, and J. TEICHMANN. Can. J. Phys. **57**, 739 (1979).
17. G. B. SESSLER. J. Acoust. Soc. Am. **42**, 360 (1967).
18. L. P. MIX, JR., L. N. LITZENBERGER, and G. BEKEFI. Phys. Fluids, **15**, 2020 (1972).
19. B. D. FRIED and S. D. CONTE. The plasma dispersion function. Academic Press, New York, NY. 1961.